Equivalent Circuit Parameters for Large Brushless Doubly Fed Machines (BDFMs)

Abdi Jalebi, S., Abdi, E., Oraee, A. & McMahon, R

Original citation & hyperlink:
Abdi Jalebi, S, Abdi, E, Oraee, A & McMahon, R 2014, 'Equivalent Circuit Parameters for Large Brushless Doubly Fed Machines (BDFM)' IEEE Transactions on Energy Conversion, vol. 29, no. 3, pp. 706715.
https://dx.doi.org/10.1109/TEC.2014.2311736

DOI 10.1109/TEC.2014.2311736
ISSN 0885-8969

Publisher: Institute of Electrical and Electronics Engineers (IEEE)

Equivalent Circuit Parameters for Large Brushless Doubly Fed Machines (BDFMs)

Salman Abdi, Ehsan Abdi, *Senior Member, IEEE,* Ashknaz Oraee, and Richard McMahon

***Abstract*— This paper presents analytical methods to calculate the equivalent circuit parameters for large-scale Brushless Doubly-Fed Machines (BDFMs) with magnetic wedges utilized for closing stator open slots. The use of magnetic wedges reduces the magnetizing currents in the machine, reflected in the values of magnetizing inductances, but also increases leakage fluxes affecting the value of series inductances in the equivalent circuit. Though such effects can be modelled by numerical models, the proposed analytical methods are particularly helpful in optimizing machine design, inverter rating, reactive power management and grid low-voltage ride-through performance. The conventional analytical methods cannot be readily applied to the BDFM due to its complex magnetic field distribution; this paper presents analytical methods to calculate the magnetizing and leakage inductances for the BDFM with magnetic wedges used in the stator slots. The proposed methods are assessed by experimentally-verified FE models for a 250 kW BDFM.**

***Index Terms*— Brushless Doubly-Fed Machine (BDFM), Finite Element (FE) method, Coupled-Circuit model, Carter factor, Magnetic wedges, Inductance calculation, Magneto Motive Force (MMF).**

I. Introduction

The BDFM is an alternative to the well-established Doubly-Fed Induction Generator (DFIG) for use in wind turbines as it retains the benefit of utilizing a fractional-size converter, but it also offers higher reliability and lower maintenance costs than the DFIG due to absence of brush gear and slip-rings [1]. In addition, the BDFM is intrinsically a medium-speed machine, enabling the use of a simplified one or two-stage gearbox, hence reducing the cost of the overall drivetrain and giving further reliability improvement.

The modern BDFM as a variable speed drive or generator comprises two electrically separate stator windings, one connected directly to the grid, called the power winding (PW), and the other supplied from a variable voltage and frequency converter, called the control winding (CW). The pole numbers are selected in a way to avoid direct transformer coupling between the stator windings and the coupling between the windings is through the rotor [2]. The rotor is specially designed to couple to the two air-gap fields associated with the two stator windings, the nested-loop design being commonly used [3]. The normal mode of BDFM operation is as a synchronous machine with the rotor rotating at a speed determined by the winding pole numbers and the mains and converter frequencies.

S. Abdi and A. Oraee and R. McMahon are with the Electrical Engineering Division, Cambridge University, Cambridge, CB3 0FA, UK (e-mail: s.abdi.jalebi@gmail.com; ashknaz.oraee@gmail.com; ram1@eng.cam.ac.uk)

E. Abdi is with Wind Technologies Limited, St Johns Innovation Park, Cambridge CB4 0WS, UK. (e-mail: ehsan.abdi@windtechnologies.com)

The equivalent circuit is a simple method of representing the steady-state performance of the BDFM, allowing the rapid calculation of operating conditions of the BDFM and its associated converter and grid connection. The equivalent circuit is also helpful for the design and optimization of the machine. The equivalent circuit parameters can be calculated from the machine geometry using the analytical methods described in [4]. They can also be extracted from BDFM steady-state operation, provided from numerical models or experimental tests, by applying curve-fitting methods [2]. Extracted parameters are likely to be more accurate as it is hard to obtain analytically precise values of certain quantities such as the leakage reactances of end-windings.

To date, there have been several attempts to manufacture large BDFMs, for example in Brazil with a 75 kW machine [5], China with the design of a 200 kW machine [6] and the 250 kW BDFM reported by the authors [7]. The latter was built in a frame size D400 as a stepping-stone towards a megawatt-scale BDFM wind turbine and it involved construction and winding techniques appropriate to large machines including magnetic wedges. These are often used in large machines with open slots [8] to reduce the effective air gap length, thereby resulting in lower magnetizing currents, which is advantageous in BDFM design. Wedges, typically comprising 75% iron powder, 7% glass mat, and 18% epoxy resin [9], also reduce core losses, and hence machine temperature rise [8], [10], [11]. On the other hand, magnetic wedges will increase the slot leakage by providing easier paths for fluxes not crossing the air gap [12].

Though the effects of magnetic wedges on the performance of induction and permanent magnet machines have been studied by others, for example in [11], [13], the methods of analysis proposed in those papers cannot be readily applied to the BDFM due to its complex design and magnetic field distribution [14]. This paper investigates the effects of magnetic wedges on the performance of the BDFM by analysing their impacts on the equivalent circuit parameters. Analytical methods are presented to calculate the magnetizing and leakage inductances for a 250 kW BDFM with magnetic wedges and Finite Element models are used to verify the accuracy of the proposed methods.

II. BDFM Equivalent Circuit Model

A simplified equivalent circuit for the BDFM is shown in Fig. 1 where all parameters are referred to the power winding side and iron losses are neglected [2]. The circuit is valid for all modes of operation, including the induction, cascade and synchronous modes and can be utilized for the analysis

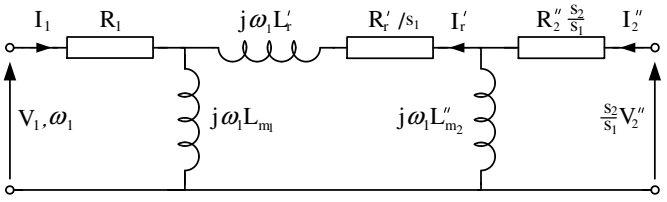

Fig. 1: Simplified equivalent circuit

of steady-state performance of the BDFM. s_1 and s_2 are the power and control winding slips and are defined as:

$$s_1 = \frac{\omega_1 - p_1\omega_r}{\omega_1} \tag{1}$$

$$s_2 = \frac{\omega_2 - p_2\omega_r}{\omega_2} \tag{2}$$

The referred rotor inductance, L'_r in the simplified circuit shown in Fig. 1 represents the series inductances in the full equivalent circuit [2], including the stator PW and CW and rotor leakage inductances. Hence, the effects of stator slot magnetic wedges on the flux leakage, will be reflected in the value of the L'_r in the simplified equivalent circuit.

As described, the equivalent circuit parameters can be calculated from the machine geometry, during the design stage, using the method described in [15]. The procedure involves deriving the machine's coupled-circuit model, followed by performing a series of transformations to obtain the d-q, sequence components and equivalent circuit parameters, respectively.

The equivalent circuit parameters can also be extracted from steady-state measures, such as torque, speed, voltages and currents, obtained from BDFM's operation in the induction and cascade modes [2]. The steady-state data can be obtained from numerical models or experimental tests. The stator winding resistances, R_1 and R_2 are either calculated from the machine geometry at a certain operating temperature or obtained from DC measurements. The magnetizing inductances L_{m1} and L_{m2} are obtained from the magnetizing tests where a single stator winding is supplied in turn whilst the other winding is left open and the rotor is driven at the synchronous speed to eliminate rotor currents. Finally, the rotor parameters L_r and R_r are obtained from applying a curve fitting method to the data from cascade tests, assuming the stator resistance and magnetizing parameters are fixed [2].

III. Models Considered in This Study

Five models have been utilized in this study to obtain the equivalent circuit parameters, which are described in Table I. Two of the models utilized are based on the coupled-circuit approach: one neglecting the effects of magnetic wedges (CC-LN-NW) and the other incorporating the authors' proposed approach to model the effects of wedges (CC-LN-W). The coupled-circuit model comprises the machine inductance and resistance matrices and the effects of iron saturation are neglected. It has been shown to give close agreement with experimental tests on a D180 size machine, for example in [17]. The inductance and resistance matrices are calculated from the machine geometry and can be transformed into the equivalent circuit parameters by performing a series of transformations [16].

The other three models are based on the 2D Finite Element (FE) approach. One assumes a linear iron circuit and no magnetic wedges (FE-LN-NW), the second one assumes a linear iron circuit and takes into account the magnetic wedges with a constant relative permeability (FE-LN-W), and the third model includes the nonlinear properties of the iron circuit and magnetic wedges(FE-NLN-W). Clearly, the latter has a significantly more computational time than the linear models, but will be shown to give the closest predictions to experimental results.

TABLE I: Different approaches utilized for obtaining the equivalent circuit parameters

Acronym	Model	Iron circuit	Magnetic wedges
CC-LN-NW	Coupled-Circuit	Linear	Not included
CC-LN-W	Coupled-Circuit	Linear	Included
FE-LN-NW	Finite Element	Linear	Not included
FE-LN-W	Finite Element	Linear	Included
FE-NLN-W	Finite Element	Non-linear	Included

IV. Prototype 250 kW D400 BDFM Specifications

A. Specifications

The specifications of the 250 kW D400 BDFM are shown in Table II. The D400 BDFM was constructed as a frame size 400 machine with the stack length of 820 mm. The stator windings were form wound from copper strips. The power winding was rated at 690 V, 178 A, at 50 Hz and the control winding was designed for 620 V at 18 Hz and rated at 73 A. Both stator windings were connected in delta. The rotor comprises six sets of nests each consisting of a number of concentric loops [18], the conductors being solid bars with one common end ring [7]. The magnetic properties for the iron and magnetic wedges were provided by the machine manufacturer.

B. Test rig and instrumentation details

Fig. 2 shows the BDFM on test bed, which was set up at the manufacturer's facility. The BDFM was driven via a torque transducer by a 355 kW 8-pole induction motor fed from a 400 kW ACS800 inverter. The PW was connected to the mains and supplied at 690 V, 50 Hz and the CW was supplied from the converter. Speed and position signals are obtained from an incremental encoder with a resolution of 10,000 pulses per revolution. The voltages and currents of each stator phase are measured by LEM AV100-750 and LEM LA 205/305-s transducers respectively. The accuracy of voltage, current, torque and speed measurements are shown in Table III, which are calculated from the specifications provided by the manufacturers and the accuracies of the conditioning circuitries.

TABLE II: Specifications of the 250 kW D400 BDFM

Frame size	400
PW pole number	4
Speed range	500 rpm ±36%
PW rated voltage	690V at 50 Hz (delta)
Rated torque	3670 Nm
PW rated current	178 A (line)
Rated power	250 kW at 680 rpm
CW pole number	8
Stack length	0.82 m
CW rated voltage	620 V at 18 Hz (delta)
Efficiency (at full load)	> 95%
CW rated current	73 A (line)

Fig. 2: 250 kW D400 BDFM (right front) on test bed

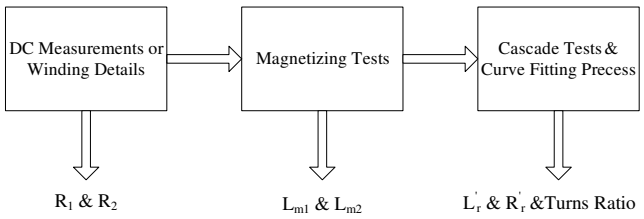

Fig. 3: Extraction of equivalent circuit parameters from numerical modelling or experimental measurements

V. Magnetizing and Cascade Tests

As described, the BDFM equivalent circuit parameters can be extracted from magnetizing and cascade tests performed by either numerical models or experiments:

A. Magnetizing tests

When only the PW or CW of the BDFM stator is supplied and the unsupplied winding is left open, the BDFM operates as a p_1 or p_2 pole pair induction machine, respectively. If the rotor speed is set to the synchronous speed using an external load machine, only the field due to the excited winding will exist in the machine and hence the equivalent circuit of Fig. 1 will reduce to only include the supplied winding's resistance and magnetizing inductance. The magnetizing inductances of PW and CW, L_{m1} and L_{m2}, can be derived from these tests.

The magnetizing characteristic of the D400 BDFM is shown in Fig. 4 for the two stator windings. Results from experiments and FE-LN-NW and FE-NLN-W models are shown. The supply frequency was 20 and 10 Hz for the PW and CW respectively.

There are two horizontal lines shown in Fig. 4: the solid line shows the rated voltage of the corresponding winding at the excited frequency and the dashed line shows the voltage at which the air gap flux is rated in the absence of the other stator field. As can be seen from Fig. 4, the effect of iron saturation is not significant below the air gap rated flux. The effect of stator slot magnetic wedges in reducing magnetizing currents is evident. The magnetizing inductances, L_{m1} and L_{m2} can be obtained from the slope of the linear region below the rated voltages.

TABLE III: Measurement Accuracy

Measurement	Total accuracy of measured value	DC Offset
Voltage	2.1%	2.3(V)
PW current	1.4%	0.5(A)
CW current	1.4%	0.3(A)
Torque	0.15%	0.1(Nm)
Speed	0.0024%	–

B. Cascade tests

The BDFM can be operated as a self-cascaded induction machine by exciting the PW or CW and shorting the other winding. A cascade induction machine formed from p_1 and p_2 pole pair induction machines has characteristics which resemble an induction machine with $p_1 + p_2$ pole pairs.

The rotor parameters, L_r and R_r and turns ratio N_1/N_2 may be obtained by applying a curve fitting method to results from BDFM cascade operation. The stator currents (both supplied and shorted windings) and torque are used for extracting the parameters. The fitting algorithm assumes fixed values for stator winding resistances and magnetizing inductances and finds values for L_r, R_r and N_1/N_2 which give the best fit. Fig. 5 shows the results from cascade tests obtained from experiments and FE-LN-NW and FE-NLN-W models. The cascade tests have been carried out at reduced voltages, i.e. PW and CW were supplied at 70 V, 20 Hz and 240 V, 20 Hz respectively, due to restrictions on stator currents, hence the extracted parameters do not represent the effect of iron saturation.

VI. Comparison of Existing Models

The equivalent circuit inductance parameters L_{m1}, L_{m2} and L_r, obtained from different modelling methods and experimen-

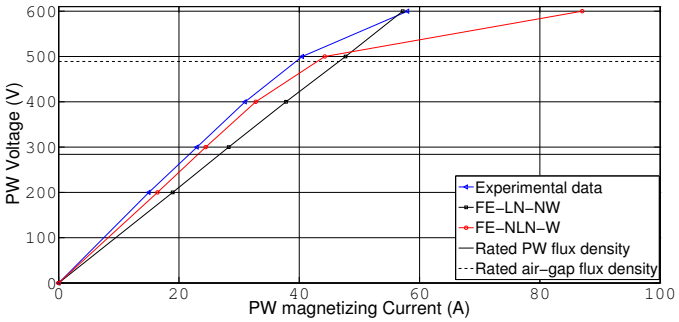

(a) Magnetizing characteristic of the stator PW.

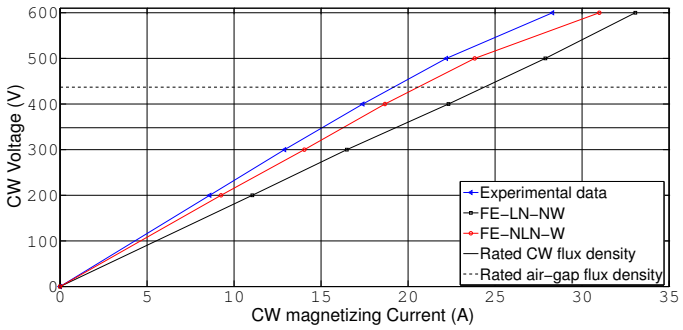

(b) Magnetizing characteristic of the stator CW.

Fig. 4: Magnetizing characteristic of the D400 BDFM

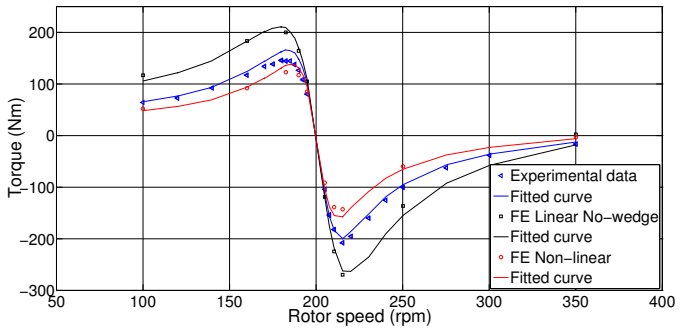

(a) Torque in PW cascade test

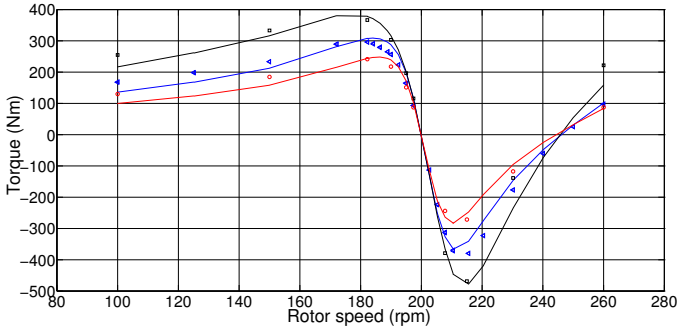

(b) Torque in PW cascade test

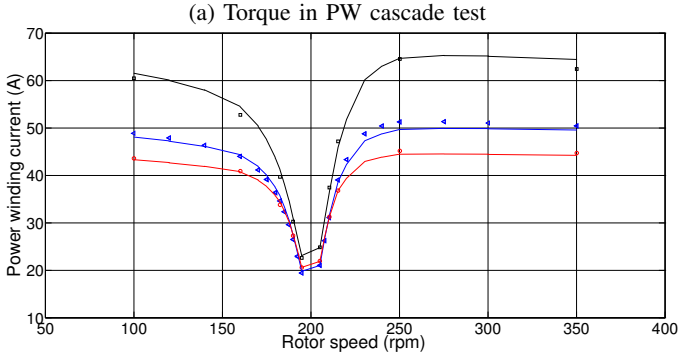

(c) I_{pw} in PW cascade test

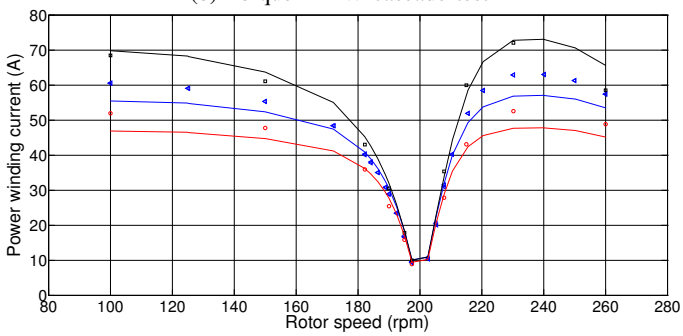

(d) I_{pw} in CW cascade test

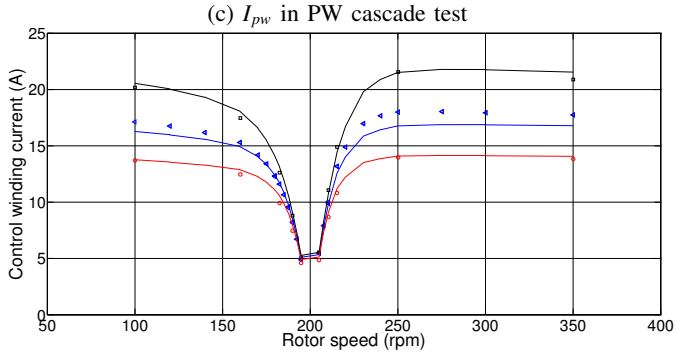

(e) I_{cw} in PW cascade test

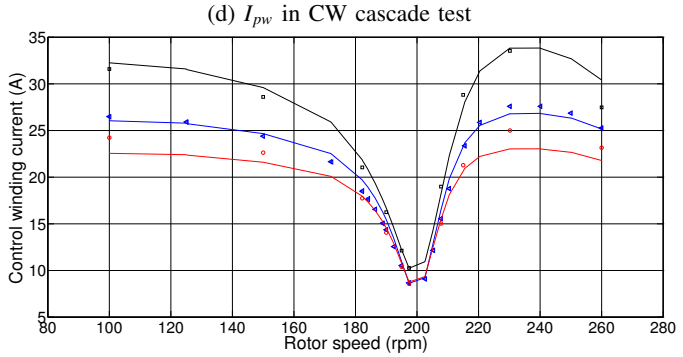

(f) I_{cw} in CW cascade test

Fig. 5: Cascade results and fitted curves for Experimental data, FE-LN-NW and FE-NLN-W models

tal tests are shown in Tables IV and V. The parameters shown in Table IV are for the machine without magnetic wedges in stator slots. The two linear models are in close agreement, as expected, which validates the assumptions used to obtain the coupled-circuit model and its transformation to equivalent circuit model proposed by Roberts in [15]. Nevertheless, neither of the models are able to take into account the effect of magnetic wedges.

Table V shows the inductance parameters obtained from FE models and experiment when magnetic wedges are considered. There is acceptable agreement between the parameters obtained from FE-NLN-W model and experiments, considering the measurement accuracies and limitations in obtaining geometrical data. There is about 15% difference in the rotor inductance L_r, mainly due to the fact that L_r represents the stator and rotor leakage inductances and the modelling of the leakage effects, for example in the case of winding overhang, is difficult. The agreement between FE-NLN-W and FE-LN-W, both using identical geometrical data, is close which shows that the non-linearity of the iron circuit can be neglected due to reduced voltage levels in the tests. It also confirms that assuming the linear magnetic property for the magnetic wedges, i.e. a constant permeability, gives acceptable accuracy.

The differences between the parameters obtained assuming no magnetic wedge in stator slots, shown in Table IV, and the ones obtained when magnetic wedges are present, shown in Table V, are significant: both magnetising and leakage inductances are larger in the latter table. Though the nonlinearity of iron circuit may also contribute in the differences, since the tests were undertaken at reduced voltage levels, such effects can be neglected.

There is therefore need for an analytical approach to model the effect of magnetic wedges in the coupled circuit model, so these effects can be considered during the design optimisation when computational cost is important. The following sections will present the authors' proposed approach.

TABLE IV: Equivalent circuit parameters without stator magnetic wedges

	L_{m1}(mH)	L_{m2}(mH)	L'_r(mH)
CC-LN-NW	82.8	282.8	9.67
FE-LN-NW	84.2	285	9.40
Difference (%)	1.4%	0.8%	2.9%

TABLE V: Equivalent circuit parameters with stator magnetic wedges

	L_{m1}(mH)	L_{m2}(mH)	L'_r(mH)
Experiment	104	368	12.45
FE-NLN-W	97.1	341	14.3
FE-LN-W	96.8	348.5	15.2

VII. Calculation of Magnetizing Inductances

The magnetizing inductances of electrical machines correspond to the magnetic flux that links the stator and rotor, passing the air gap twice. The effects of stator and rotor slotting in the magnetizing inductance are often modelled by Carter factors which effectively scale the air gap length. The effect of magnetic wedges in reducing magnetizing currents, hence increasing magnetizing inductances, can also be modelled by scaling the air gap length, similar to the concept of Carter factors [19]. Hence, modified Carter factors may be derived which can take into account the effect of both slotting and magnetic wedges.

The Carter factor is effectively the ratio of the air gap peak flux density, which would be the case in the absence of slotting, and its average value when slotting is considered [20]. When both rotor and stator have open slots, it is assumed that the resultant Carter factor is the product of the Carter factors for the stator and rotor [21]. Since magnetic wedges are only used in stator slots of the BDFM, the following presents the calculation of Carter factor for the stator assuming an un-slotted rotor using the magnetic equivalent circuit (MEC) method. The Carter factor for the rotor can be calculated using conventional methods described, for example, in [21]. The following assumptions are made:

- There is no saturation in the iron circuit and in magnetic wedges and hence infinite and constant permeabilities are assumed for iron and magnetic wedges, respectively.
- The magnetic wedges are assumed to have a rectangular shape.
- There are three magnetic paths between the stator tooth and un-slotted rotor, through which magnetic fluxes ϕ_t, ϕ_o and ϕ_w enter the rotor as shown in Fig. 6. Θ is considered as the total MMF that produces these fluxes.
- The reluctance between the above mentioned magnetic paths is infinite and hence the interaction between their corresponding magnetic fluxes is negligible.

A typical variation of air gap flux density over a slot pitch is shown in Fig. 6 with presence of a magnetic wedge, where B_{av}, B_{max} and B_{min} are average, maximum and minimum air gap flux densities, respectively.

The reluctances associated with magnetic paths corresponding to ϕ_o and ϕ_w include:

$$R_{ox} = \frac{x}{\mu_0 A_{ox}}, R_{oy} = \frac{y}{\mu_0 A_{oy}}, R_{og} = \frac{g}{\mu_0 A_{og}}, \tag{3}$$

$$R_{wx} = \frac{x}{\mu_0 \mu_w A_{wx}}, R_{wy} = \frac{y}{\mu_0 \mu_w A_{wy}}, R_{wg} = \frac{g+d}{\mu_0 A_{wg}}, \tag{4}$$

Where g is the air gap length, d is the depth of air-filled region above the magnetic wedge, μ_w is the relative permeability of the magnetic wedge and A is the area through which the magnetic flux is passing. The flux entering the rotor consists of three fluxes: ϕ_w, ϕ_o and ϕ_t shown in Fig. 6. B_{wx}, B_{wy}, B_{ox} and B_{oy} are the flux densities associated to reluctances R_{wx}, R_{wy}, R_{ox} and R_{oy} respectively. Assuming Θ is the MMF producing ϕ_w, ϕ_o and ϕ_t, and the MMF across R_{wx}, R_{wy}, R_{wg} and R_{ox}, R_{oy}, R_{og} are Θ_{wx}, Θ_{wy}, Θ_{wg} and Θ_{ox}, Θ_{oy}, Θ_{og} respectively, the following equations can be obtained:

$$\Theta = \Theta_{ox} + \Theta_{oy} + \Theta_{og} = \Theta_{wx} + \Theta_{wy} + \Theta_{wg} \tag{5}$$

$$\Theta = R_{ox} A_{ox} B_{ox} + (R_{oy} A_{oy} + R_{og} A_{og}) B_{oy} \tag{6}$$

$$\Theta = R_{wx} A_{wx} B_{wx} + (R_{wy} A_{wy} + R_{wg} A_{wg}) B_{wy} \tag{7}$$

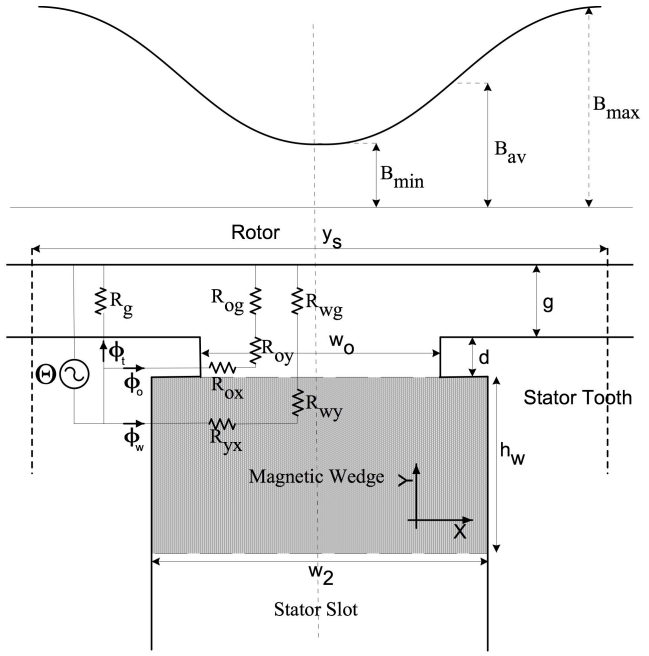

Fig. 6: Different magnetic paths from stator tooth to the rotor

Along the path R_{ox} and R_{oy}, the area through which ϕ_o is traveling can be assumed uniform, i.e. A_{ox}=A_{oy}, hence:

$$B_{ox} = B_{oy} \tag{8}$$

Considering the path for ϕ_w, the flux densities B_{wx} and B_{wy} are related as:

$$B_{wx} = B_{wy}\frac{w_o}{2h_w} \tag{9}$$

From (6) to (9) and since R_{oy} and R_{wy} are negligibly small,

$$\Theta = B_{oy}\frac{x+g}{\mu_0} = B_{wy}(\frac{w_o x}{2\mu_0\mu_w h_w} + \frac{g+d}{\mu_0}) \tag{10}$$

Hence:

$$B_{oy} = \frac{\mu_0\Theta}{x+g} \tag{11}$$

$$B_{wy} = \frac{\Theta}{\frac{w_o}{2\mu_0\mu_w h_w}x + \frac{g+d}{\mu_0}} \tag{12}$$

The magnetic fluxes ϕ_o and ϕ_w can be worked out from the flux densities B_{oy} and B_{wy} as:

$$\phi_o = \int_0^d B_{oy}.dx = \mu_0\Theta\ln(\frac{g+d}{g}) \tag{13}$$

$$\phi_w = \int_0^{\frac{w_2}{2}} B_{wy}.dx = \frac{2h_w\mu_0\mu_w\Theta}{w_o}\ln(\frac{\frac{w_o w_2}{4h_w}}{\mu_w(g+d)}) \tag{14}$$

Where w_o and w_2 correspond to the stator slot opening width and magnetic wedge width respectively, as shown in Fig. 6. Considering $B_{max-airgap}$ corresponds to the magnetic flux ϕ_{max} passing through the air gap for an unslotted stator, the air gap correction factor for taking magnetic wedges into account can be derived as:

$$K_{c-stator} = \frac{B_{max-airgap}}{B_{mean-airgap}} = \frac{\phi_{max}}{\phi_t + 2(\phi_o + \phi_w)} \tag{15}$$

Where

$$\phi_{max} = \frac{\mu_0 y_s\Theta}{g} \tag{16}$$

$$\phi_t = \frac{\mu_0(y_s - w_o)\Theta}{g} \tag{17}$$

Substituting Equations (13), (14), (16) and (17) in Equation (15) give

$$K_{c-stator} = \frac{y_s}{(y_s - w_2) + \frac{4h_w g}{w_o}\mu_w\ln\{\frac{\frac{w_o w_2}{4h_w} + \mu_w(g+d)}{\mu_w(g+d)}\} + 2g\ln(\frac{g+d}{g})} \tag{18}$$

The rotor Carter factor $k_{c-rotor}$ is calculated for the D400 BDFM using the method proposed by [21]:

$$k_{c-rotor} = \frac{y_r + 8g}{y_r - w_r + 8g} \tag{19}$$

Where y_r is the rotor slot pitch and w_r is the rotor slot opening width. Equation 19 has empirical justification and is valid when $\frac{w_o}{g}$ is not sufficiently large (less than 12) [21]. The overall effective air gap g_e can be calculated using the product of stator and rotor Carter factors [22]:

$$g_e = g \times k_{c-stator} \times k_{c-rotor} \tag{20}$$

The effective air gap can be used in the calculation of magnetising inductances for the BDFM. The validity of the proposed method will be verified in Section IX using numerical analysis.

VIII. Calculation of Leakage Inductances

Inductance arising from leakage effects are inductances due to the magnetic flux not linking stator and rotor conductors. This definition is similar to that found in [23], except that for the purposes of this paper, the harmonic mutual inductance terms are not considered part of the leakage terms, rather as a separate term.

The calculation of stator and rotor winding leakage inductances is greatly simplified by the calculation of specific permeance which is defined as the self-inductance per unit length of coil per turn squared. Thus, to calculate the self-inductance of a coil due to leakage, the different permeance terms around the length of the coil should be summed and the result multiplied by the number of turns squared. Consequently, the per phase leakage inductances for stator PW and CW, L_{s-pw} and L_{s-cw} can be calculated:

$$L_{s-pw} = C_{pw}N_{pw}^2\ell'\lambda_{s-pw} \tag{21}$$

$$L_{s-cw} = C_{cw}N_{cw}^2\ell'\lambda_{s-cw} \tag{22}$$

Where C_{pw} and C_{cw} are the PW and CW number of coils per phase, N_{pw} and N_{cw} are the number of turns per coil, λ_{s-pw} and λ_{s-cw} are the specific permeances and ℓ' is the stator effective stack length. There are four major sources of leakage permeance in induction machines [22]–[24], which are also taken into account for the BDFM: slot permeance, tooth-top permeance, overhang permeance and zig-zag permeance. Among the leakage terms, the slot leakage in most cases has the largest contribution in the winding leakage.

As shown in Section VI, there is a large discrepancy in the value of L'_r when the effects of magnetic wedges are ignored. This is most likely due to easier paths for stator leakage fluxes in the stator slot openings enabled by the magnetic wedges. The other leakage terms as well as the rotor leakage are assumed to be largely unaffected by stator wedges. The following presents the calculations of slot permeance when magnetic wedges are used in stator slot openings. The slot contains two stator windings, the PW and CW, and each winding is assumed to have a double-layer arrangement that is a common practice in large electrical machines. Derivations according to [23] are used for the other permeance terms.

Fig. 7 shows the stator slot. The slot leakage for the PW is calculated here; a similar approach can be used to derive the CW slot leakage. The slot permeance of the PW can be obtained by calculating the energy of the leakage magnetic field in a slot:

$$W_\phi = \sum_{i=1}^{7} \frac{1}{2\mu_i} \oint_{v_i} B_i^2(h).dv_i \tag{23}$$

where

$$B(h) = \begin{cases} B_1(h) = \mu_1 \frac{\Theta_{pw-A} \frac{h}{h_{pw}}}{w_1}, & 0 < h < h_{pw}, \\ B_2(h) = \mu_2 \frac{\Theta_{pw-A}}{w_1}, & h_{pw} < h < h_1, \\ B_3(h) = \mu_3 \frac{\Theta_{pw-A} + \Theta_{pw-B} \frac{h-h_1}{h_{pw}}}{w_1}, & h_1 < h < h_2, \\ B_4(h) = \mu_4 \frac{\Theta_{pw-A} + \Theta_{pw-B}}{w_1}, & h_2 < h < h_3, \\ B_5(h) = \mu_5 \frac{\Theta_{pw-A} + \Theta_{pw-B}}{w_2}, & h_3 < h < h_4, \\ B_6(h) = \mu_6 \frac{\Theta_{pw-A} + \Theta_{pw-B}}{w_2 + (w_o - w_2)\frac{h-h_4}{h_{w_1}}}, & h_4 < h < h_5, \\ B_7(h) = \mu_7 \frac{\Theta_{pw-A} + \Theta_{pw-B}}{w_o}, & h_5 < h < h_6, \end{cases}$$

and

$$dv_1 = dv_2 = dv_3 = dv_4 = \ell'.w_1.dh \tag{24}$$

$$dv_5 = \ell'.w_2.dh \tag{25}$$

$$dv_6 = \ell' \left[w_2 + (w_o - w_2)\frac{h}{h_{w_1}} \right].dh \tag{26}$$

$$dv_7 = \ell' w_o.dh \tag{27}$$

$$\mu_1 = \mu_2 = \mu_3 = \mu_4 = \mu_7 = \mu_0 \tag{28}$$

$$\mu_5 = \mu_6 = \mu_w \tag{29}$$

ℓ' is the stator effective stack length and Θ_{pw-A} and Θ_{pw-B} are the total current linkages of the PW bottom and upper layers. All different heights and widths are specified in Fig. 7. The energy of the PW leakage magnetic field in the slot from (23) is:

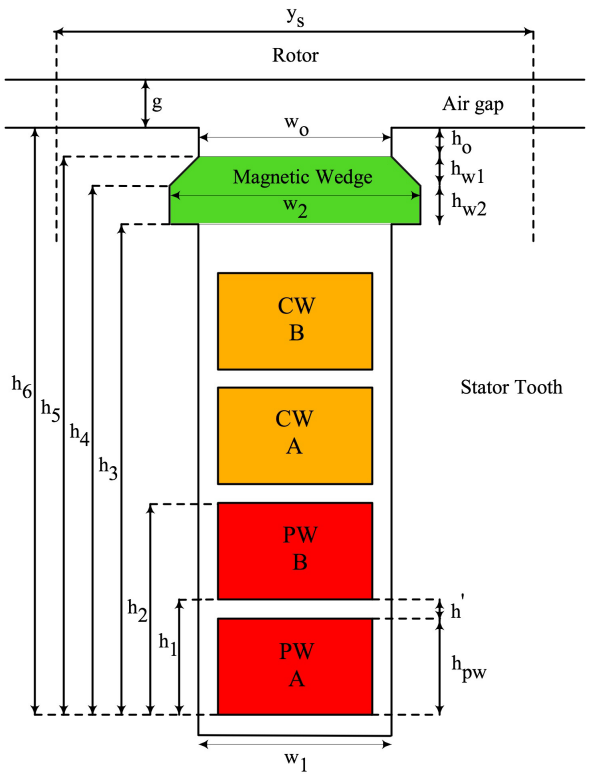

Fig. 7: D400 BDFM stator slot details

$$\begin{aligned} W_\phi = \; & \frac{\ell'\mu_0}{2w_1}[\Theta_{pw-A}^2 \int_0^{h_{pw}} (\frac{h}{h_{pw}})^2.dh + \Theta_{pw-A}^2 \int_{h_{pw}}^{h_1} dh + \\ & \int_{h_1}^{h_2} (\Theta_{pw-A} + \Theta_{pw-B}\frac{h-h_1}{h_{pw}})^2.dh + \\ & (\Theta_{pw-A} + \Theta_{pw-B})^2 \int_{h_2}^{h_3} .dh] + \\ & \frac{\ell'\mu_w}{2w_2}(\Theta_{pw-A} + \Theta_{pw-B})^2 \int_{h_3}^{h_4} dh + \frac{\ell'\mu_0}{2w_0} \int_{h_4}^{h_5} dh + \\ & \frac{\ell'\mu_w}{2}(\Theta_{pw-A} + \Theta_{pw-B})^2 \int_{h_5}^{h_6} \frac{dh}{w_2 + (w_o - w_2)\frac{h-h_5}{h_{w_1}}} \end{aligned} \tag{30}$$

Note that:

$$\Theta_{pw-A} = \Theta_{pw-B} = \frac{1}{2}\Theta_{pw} \tag{31}$$

When a short pitched winding is used, the currents in the two CW coils in a stator slot are either in phase or have a 120° phase shift. In case of the latter, the term $\Theta_{pw-A}.\Theta_{pw-B}$ in (30) is multiplied by $\cos\frac{2\pi}{3}$, representing the mutual influence of the bottom and upper currents [22]. Assuming q is the number of slots per phase per pole and a is the number of short pitched slots, the *cos* terms can be averaged as:

$$\cos\beta = \frac{1}{2q}\sum_{i=1}^{2q} \cos\gamma_i = \frac{1}{2q}\left[2a\cos\frac{2\pi}{3} + 2(q-a)\cos 0\right] \tag{32}$$

The term $\Theta_{pw-A}.\Theta_{pw-B}$ can hence be written as:

$$\Theta_{pw-A}.\Theta_{pw-B} = \Theta_{pw}^2 \cos\beta_{pw} \tag{33}$$

Substituting (32) and (33) into (30), the PW leakage magnetic field energy in the slot is:

$$W_\phi = \frac{1}{2}\ell'\Theta_{pw}^2\mu_0\left[(\frac{5}{3}+\cos\beta_{pw})\frac{h_{pw}}{w_1}+\frac{h'}{w_1}+\frac{h_3-h_2}{w_1}(2+2\cos\beta_{pw})+\frac{h_o}{w_o}(2+2\cos\beta_{pw})\right]+\frac{1}{2}\ell'\Theta_{pw}^2\mu_w\left[\frac{h_{w_2}}{w_2}(2+2\cos\beta_{pw})+\frac{h_{w_1}}{w_2-w_o}(2+2\cos\beta_{pw})\ln(\frac{w_2}{w_o})\right] \quad (34)$$

The total PW leakage magnetic energy stored in the slot is:

$$W_\phi = \frac{1}{2}L_{slot-leakage}\Theta_{pw}^2 = \frac{1}{2}\ell'\Theta_{pw}^2\lambda_{s-pw} \quad (35)$$

Where λ_{s-pw} is the PW slot leakage of one slot. From (34) and (35), λ_{s-pw} can be extracted by defining three terms: self-permeance for PW layer A λ_{pw-A}, layer B λ_{pw-B}, and mutual permeance between these two layers λ_{pw-M}:

$$\lambda_{pw-A} = \mu_0(\frac{h_{pw}}{3w_1}+\frac{h_3-h_{pw}}{w_1}+\frac{h_o}{w_o})+\mu_w(\frac{h_{w_2}}{w_2}+\frac{h_{w_1}}{w_2-w_o}\ln(\frac{w_2}{w_o})) \quad (36)$$

$$\lambda_{pw-B} = \mu_0(\frac{h_{pw}}{3w_1}+\frac{h_3-h_2}{w_1}+\frac{h_o}{w_o})+\mu_w(\frac{h_{w_2}}{w_2}+\frac{h_{w_1}}{w_2-w_o}\ln(\frac{w_2}{w_o})) \quad (37)$$

$$\lambda_{pw-M} = \mu_0(\frac{h_{pw}}{2w_1}+\frac{h_3-h_2}{w_1}+\frac{h_o}{w_o})+\mu_w(\frac{h_{w_2}}{w_2}+\frac{h_{w_1}}{w_2-w_o}\ln(\frac{w_2}{w_o})) \quad (38)$$

λ_{s-pw} is then:

$$\lambda_{s-pw} = \lambda_{pw-A}+\lambda_{pw-B}+2\times\lambda_{pw-M}\times\cos\beta_{pw} \quad (39)$$

The slot leakage for the CW can be derived using the same procedure as that of presented for the PW as:

$$\lambda_{s-cw} = \lambda_{cw-A}+\lambda_{cw-B}+2\times\lambda_{cw-M}\times\cos\beta_{cw} \quad (40)$$

The PW and CW leakage inductances can now be calculated from (21) and (22).

IX. Verification of Analytical Methods

In order to verify the accuracy of the proposed analytical methods in Sections VII and VIII, the magnetising and leakage inductances derived from the coupled circuit model embedding the new analytical methods are compared with parameters predicted by the numerical models, i.e. FE-LN-W.

Fig. 8 shows the area in the stator slot opening which is occupied by a magnetic wedge. Three cases have been considered to examine the accuracy of the analytical methods with respect to wedge dimensions and permeability, see Table VI:

Case A: this is the real case in the D400 BDFM. The magnetic wedge fills *Area*1 and *Area*2 and has a relative permeability of $\mu_w = 20$ which is an approximation of its non-linear magnetic characteristic provided by the manufacturer.

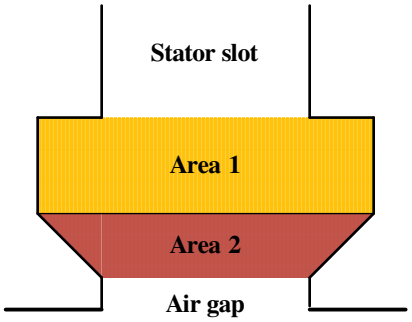

Fig. 8: Areas covered with magnetic wedges for different cases

Case B: the magnetic wedge has identical dimensions as Case A, but its relative permeability is assumed to be $\mu_w = 10$.

Case C: the magnetic wedge only fills *Area*1 and hence *Area*2 is assumed unfilled i.e. is filled by air. The relative permeability of magnetic wedge is identical to Case A, i.e. $\mu_w = 20$.

TABLE VI: Dimensions and relative permeability of magnetic wedges used for verification of analytical methods

	Magnetic Wedge	
	μ_w	Area
Case A	20	Area1 & Area2
Case B	10	Area1 & Area2
Case C	20	Area1

The magnetizing and leakage inductance parameters in the referred equivalent circuit shown in Fig. 1 are calculated using the coupled circuit and FE-LN-W models for Cases A, B and C and are shown in Tables VII, VIII and IX. As can be seen, there is generally close agreement between the parameters predicted by two models for all the three cases, hence validating the proposed analytical methods. The difference in the magnetizing inductances is below 2% in all cases which confirms that the proposed method to calculate the Carter factor used to obtain an effective air gap length leads to acceptable accuracy.

The difference in L_r which represents the stator and rotor leakage inductances is around 4 to 5 %, well within the limitations of calculating leakage fluxes. The prediction of leakage inductance by the coupled circuit model in all three cases is always higher than the numerical model, showing that the analytical method overestimates the leakage inductances.

An important conclusion from the results shown in Tables VII, VIII and IX is that, the differences in the parameters calculated from analytical and numerical methods are small and, for all the three cases, are in a similar range; this confirms the accuracy of the analytical methods with respect to dimensions and magnetic property of magnetic wedges. Thus, the approach can be utilized during the BDFM design

optimization to specify suitable magnetic wedges for stator slot openings in order to achieve an appropriate balance between the magnetization requirements, reactive power management and low-voltage ride-through performance of the machine.

TABLE VII: Equivalent circuit parameters Case A

	L_{m1}(mH)	L_{m2}(mH)	L'_r(mH)
FE-LN-W	96.8	348.5	15.2
CC-LN-W	98.3	352	16
Difference (%)	1.5%	1%	5.2%

TABLE VIII: Equivalent circuit parameters Case B

	L_{m1}(mH)	L_{m2}(mH)	L'_r(mH)
FE-LN-W	93	329.2	12.3
CC-LN-W	94.6	330	12.8
Difference (%)	1.7%	0.2%	4.1%

TABLE IX: Equivalent circuit parameters Case C

	L_{m1}(mH)	L_{m2}(mH)	$L'_r(mH)$
FE-LN-W	90	319.4	12.8
CC-LN-W	91.7	323	13.4
Difference (%)	1.9%	1.1%	4.7%

X. Conclusions

In this paper, the equivalent circuit parameters have been derived for a 250 kW D400 BDFM using several methods including analytical and numerical models and from experimental tests. One key feature of this BDFM as compared to the ones studied before is the use of magnetic wedges in stator slot openings, which affect the magnetising properties of the machine as well as reactive power management and performance during grid low voltage faults. The use of magnetic wedges in large electrical machines is common and is expected to be utilized in large BDFMs, and hence the approach of this paper is important.

It was shown that existing analytical methods are not able to give acceptable accuracy in calculating magnetizing and leakage inductances for the BDFM with magnetic wedges used in stator slots. Hence, analytical methods have been proposed to take into account the effects of magnetic wedges. A modified Carter factor has been derived which is used to calculate the effective air gap length to obtain the magnetizing inductances in the BDFM. In addition, a method to calculate slot leakages has been presented which calculates the increase in stator leakage inductances due to the presence of magnetic wedges. The analytical methods have been used to predict the parameter values for the D400 BDFM and two other design variations with magnetic wedges of different dimensions and magnetic property and results have been compared to predictions from numerical models. It has been shown that the analytical methods lead to good agreement with numerical models, hence have sufficient accuracy to be used in the BDFM design optimisation.

Acknowledgment

The research leading to these results has received funding from the European Union's Seventh Framework Program managed by REA Research Executive Agency (FP7/2007 2013) under Grant Agreement N.315485.

References

[1] H. Arabian-Hoseynabadi, H. Oraee, and P. J. Tavner, "Wind turbine productivity considering electrical subassembly reliability," *Renewable Energy*, no. 35, pp. 190–197, 2010.

[2] P. C. Roberts, R. A. McMahon, P. J. Tavner, J. M. Maciejowski, and T. J. Flack, "Equivalent circuit for the brushless doubly fed machine (bdfm) including parameter estimation and experimental verification," *Electrical Power Applications, IEE Proceedings*, vol. 152, no. 4, pp. 933–942, July 2005.

[3] R. A. McMahon, X. Wang, E. Abdi-Jalebi, P. J. Tavner, P. C. Roberts, and M. Jagiela, "The bdfm as a generator in wind turbines." 12th International Power Electronics and Motion Control Conference, EPE-PEMC, September 2006.

[4] R. McMahon, P. Tavner, E. Abdi, P. Malliband, and R. McMahon, "Characterising rotors for brushless doubly-fed machines (bdfm)." Rome: International Conference on Electrical Machines (ICEM), 2010, pp. 3501 – 3508.

[5] R. Carlson, H. Voltolini, F. Runcos, P. Kuo-Peng, and N. Baristela, "Performance analysis with power factor compensation of a 75 kw brushless doubly fed induction generator prototype." IEEE International Conference on Electric Machines and Drives, 2010.

[6] H. Liu and L. Xu, "Design and performance analysis of a doubly excited brushless machine for wind power generator application." IEEE International Sympousiom on Power Electronics for Distributed Generation Systems, 2010, pp. 597 – 601.

[7] R. A. McMahon, E. Abdi, P. Malliband, S. Shao, M. E. Mathekga, and P. J. Tavner, "Design and testing of a 250 kw brushless dfig." Bristol, UK: 6th IET International Conference on Power Electronics, Machines and Drives (PEMD), March 2012.

[8] Y. Takeda, T. Yagisawa, and M. Yamamoto, "Application of magnetic wedges to large motors," *IEEE Transactions on Industry Applications*, vol. MAG-20, no. 5, pp. 1780 – 1782, 1984.

[9] R. A. Hanna, W. Hiscock, and P. Klinowski, "Failure analysis of three slow-speed induction motors for reciprocating load application," *IEEE Transactions on Industry Applications*, vol. 43, no. 2, pp. 429 – 435, 2007.

[10] A. Kaga, Y. Anazawa, H. Akagami, S. Watabe, and M. Makino, "A research of efficiency improvement by means of wedging with soft ferrite in small induction motor," *IEEE Transactions on Magnetics*, vol. MAG-18, no. 6, pp. 1547 – 1549, 1982.

[11] J. Kappatou, C. Gyftakis, and A. Safacas, "A study of the effects of the stator slot wedges material on the behaviour of an induction machine." Portugal: International Conference on Electrical Machines, 2008.

[12] S. Wang, Z. Zhao, L. Yuan, and B. Wang, "Investigation and analysis of the influences of magnetic wedges on high voltage motors performance." Harbin, China: IEEE Vehicle Power and Propulsion Conference (VPPC), September 2008.

[13] G. Donato, F. Capponi, and F. Caricchi, "No-load performance of axial flux permanent magnet machines mounting magnetic wedges," *IEEE Transactions on Industrial Electronics*, vol. 59, no. 10, pp. 3768 – 3779, 2012.

[14] E. Abdi, P. Malliband, and R. McMahon, "Study of iron saturation in brushless doubly-fed induction machines." Atlanta: Energy Conversion Congress and Exposition (ECCE), November 2010, pp. 3501 – 3508.

[15] P. C. Roberts, "A study of brushless doubly-fed (induction) machines," Ph.D. dissertation, University of Cambridge, 2005.

[16] E. Abdi, "Modelling and instrumentation of brushless doubly-fed (induction) machines," Ph.D. dissertation, University of Cambridge, 2006.

[17] E. Abdi, X. Wang, S. Shao, R. A. McMahon, and P. Tavner, "Performance characterisation of brushless doubly-fed generator." Edmonton, Canada: 2008 IEEE Industry Applications Society Annual Meeting, October 2008, pp. 1 – 6.

[18] R. McMahon, P. Tavner, E. Abdi, P. Malliband, and D. Barker, "Characterising brushless doubly fed machine rotors," *IET Electric Power Applications*, vol. 7, pp. 535 – 543, 2013.

[19] P. Neti and S. Nandi, "Determination of effective air-gap length of reluctance synchronous motors from experimental data." IEEE Industry Applications Conference (IAS), October 2004, pp. 86 – 93.

[20] F. W. Carter, "Note on air gap and interpolar induction," *Institute of Electrical Engineers Journal*, vol. 29, 1900.
[21] B. Heller and V. Hamata, *Harmonic Field Effects in Induction Machines*. Elsevier Scientific Publishing Company, 1977.
[22] J. Pyrhonen, T. Jokinen, and V. Hrabovcova, *Design of rotating electrical machines*. Finland: John Wiley & Sons Inc., 2007.
[23] A. Draper, *Electrical Machines*, 2nd ed. Longmans, 1981.
[24] G. S. Brosan and J. T. Hayden, *Advanced Electrical Power and Machines*. London: Sir Isaac Pitman & Sons Ltd., 1966.

Salman Abdi received his BSc degree from Ferdowsi University, Mashhad, Iran, in 2009 and M.S.c degree from Sharif University of Technology in 2011. He is currently working toward the PhD degree at Cambridge University in electrical machines design and modelling. His main research interests include electrical machines and drives for renewable power generation

Ehsan Abdi received his BSc degree from Sharif University of Technology in 2002 and his MPhil and PhD degrees from Cambridge University in 2003 and 2006 respectively, all in Electrical Engineering. Currently, he is the Managing Director of Wind Technologies Ltd where he has been involved with commercial exploitation of the brushless doubly fed induction generator technology for wind power applications. His main research interests include electrical machines and drives, renewable power generation, and electrical measurements and instrumentation.

Ashknaz Oraee received her B.Eng. degree from Kings College London 2011. She is currently working toward the PhD degree at Cambridge University in electrical machine design and optimisation. Her research interests include electrical machines and drives for renewable power generation.

Richard McMahon received the degrees of BA (in Electrical Sciences) and PhD from Cambridge University in 1976 and 1980 respectively. Following postdoctoral work on semiconductor device processing he was appointed University Lecturer in Electrical Engineering at Cambridge University Engineering department in 1989 and became a Senior Lecturer in 2000. His research interests include electrical drives, power electronics and semiconductor materials.